Available online at www.sciencedirect.com
SCIENCE DIRECT®
Journal of Power Sources 139 (2005) 261–268
JOURNAL OF POWER SOURCES
www.elsevier.com/locate/jpowsour

Kinetic analysis of the Li^+ ion intercalation behavior of solution derived nano-crystalline lithium manganate thin films

S.R. Das, S.B. Majumder, R.S. Katiyar*

Department of Physics, University of Puerto Rico, San Juan, PR 00931-3343, USA

Received 27 May 2004; accepted 28 June 2004
Available online 24 August 2004

Abstract

In the present work, we have optimized the process parameters to synthesize nano-crystalline lithium manganate (LMO) thin films with dense surface morphology and uniform grain size distribution by a solution growth technique. These films were characterized in terms of their phase formation, surface morphology, charge–discharge capacity, rate capability, and cycleability. The films exhibited excellent discharge capacity (close to the theoretical capacity of LMO) and rate capability in a wide range of discharge current densities. However, the rapid capacity fading was observed within the first few initial charge–discharge cycles and with progressive cycling marginal capacity fading was observed. To understand these phenomena, we have investigated the kinetics of Li ion diffusion in these thin film electrodes by cyclic voltammetry (CV) as well as potential step chronoamperometry (PSCA) measurements. In case of the cycled thin film electrode, the Li ion diffusion coefficient was reduced to almost one order of magnitude as compared to its virgin counterpart. During the charge–discharge cycling of these thin film electrodes in a liquid electrolyte, a surface electrolyte interface (SEI) layer was formed on the thin film electrode. It has been argued that the formation of such layer would reduce the Li ion diffusion coefficient and led to the observed capacity fading.

Keywords: Lithium manganate; Sol–gel; Thin film; Kinetic analysis

1. Introduction

Lithium manganate (LMO) is one of the most attractive cathode materials for Li ion rechargeable batteries due to its relatively higher energy density, environmentally benign nature, and lower material cost [1]. For efficient performance of the battery, the Li^+ diffusion into the intercalating electrodes must be high. Faster Li^+ diffusion in the electrode materials would certainly improve the rate capabilities of Li ion batteries. In this regard, the development of nano-structured electrodes is attractive [2,3]; since in such electrodes, Li^+ diffusion distance is reduced considerably and faster diffusion yields better electrochemical performance of the electrode materials. Moreover, the nano-size particles have large surface area to volume ratio; therefore, the effective charge transfer is also expected to be superior. Extensive investigations on the LMO cathode were performed using micro-meter size particles and their electrochemical properties were optimized for practical applications [4,5]. Recently several research efforts were made to synthesize nano-crystalline LMO particles. From these studies, it is not clear whether the use of nano-size LMO cathode would have any distinct beneficiary effect over their micron size counterparts [6–9]. Possibly the kinetics of the intercalation behavior of Li^+ ions in nano-size LMO are intrinsically different as compared to their micro-crystalline counterpart or the particle agglomeration during electrode preparation barred any possible size effect.

Usually the electrochemical properties of LMO have been evaluated in the form of porous composite electrodes made out of LMO (as active element), carbon black (as conducting agent), and binder material (e.g. polyvinylidene fluoride). Studies on the kinetics of Li^+ insertion/extraction processes in LMO electrodes are quite limited. It is difficult to obtain re-

* Corresponding author. Tel.: +1 787 751 4210; fax: +1 787 764 2571.
E-mail address: rkatiyar@rrpac.upr.clu.edu (R.S. Katiyar).

0378-7753/$ – see front matter © 2004 Elsevier B.V. All rights reserved.
doi:10.1016/j.jpowsour.2004.06.056

liable kinetic information from the analyzed electrochemical data of the composite electrodes due to the interference of the additives as well as their porous morphology [10,11]. To obtain reliable kinetic information of Li ion diffusion, potential step chronoamperometry (PSCA), potential intermittent titration technique (PITT), and electrochemical impedance spectroscopy (EIS) measurements were performed on $LiMn_2O_4$ single crystals, thin films, and single polycrystalline particles. In a recent report, Dokko et al. [12] compared the apparent chemical diffusion coefficients of Li ion in single crystal, thin film, and single polycrystalline particles (diameter 8–21 μm) of $LiMn_2O_4$. The diffusion coefficients of single crystals and thin films were reported to be about one order of magnitude smaller than the single polycrystalline particles which was in fact the aggregates of several smaller particles. Higher diffusion coefficients in the polycrystalline particles seem to be due to better Li ion transfer within the grain boundaries of the polycrystalline aggregates. It is also reported that the lithium intercalation is easier at the surface than at the core of the grain; and therefore, larger the surface area higher is the specific capacity of the cathode material [13]. Viewing in the light of these reports, $LiMn_2O_4$ thin films with nano-size grains with homogeneous size distribution are considered to be ideal systems to study the Li ion diffusion kinetics. The nano-grain size is expected to reduce the Li ion diffusion distance and at the same time the higher grain boundary concentration would provide better Li ion intercalation to improve the electrochemical characteristics of these thin films. With the progressive miniaturization, the current and power requirements of the micro-electronic devices have been reduced to extremely low level. Therefore, from the technological point of view also the studies of thin film micro-batteries are needed to be actively pursued to be used as power sources for some of these devices [14].

In the present work, we have synthesized dense, nanocrystalline LMO thin films by a cost effective chemical solution deposition technique. By optimizing the deposition parameters and heat treatment schedule, we obtained dense, nano-size, and cubic spinel lithium manganate thin films with narrow grain size distribution. Since in thin film form, no additional secondary material (e.g. binder, and conducting agent) was added, we could investigate only the characteristics of LMO and at the same time the uncertainty associated with porous electrode to measure the kinetics of Li^+ intercalation was also avoided. These films exhibited excellent discharge capacity (close to the theoretical limit of LMO) in the cut of voltage range of 4.2–3.4 V and discharge current densities ranging 30–180 $\mu Ah\,cm^{-2}$. However, rapid capacity fading was observed within the first few charge–discharge cycles followed by a marginal capacity loss with additional charge–discharge cycles. To understand the initial rapid capacity fading of these nano-crystalline thin films, the diffusion coefficient of Li^+ was estimated from the cyclic voltammetry (CV) as well as PSCA measurements. It was found

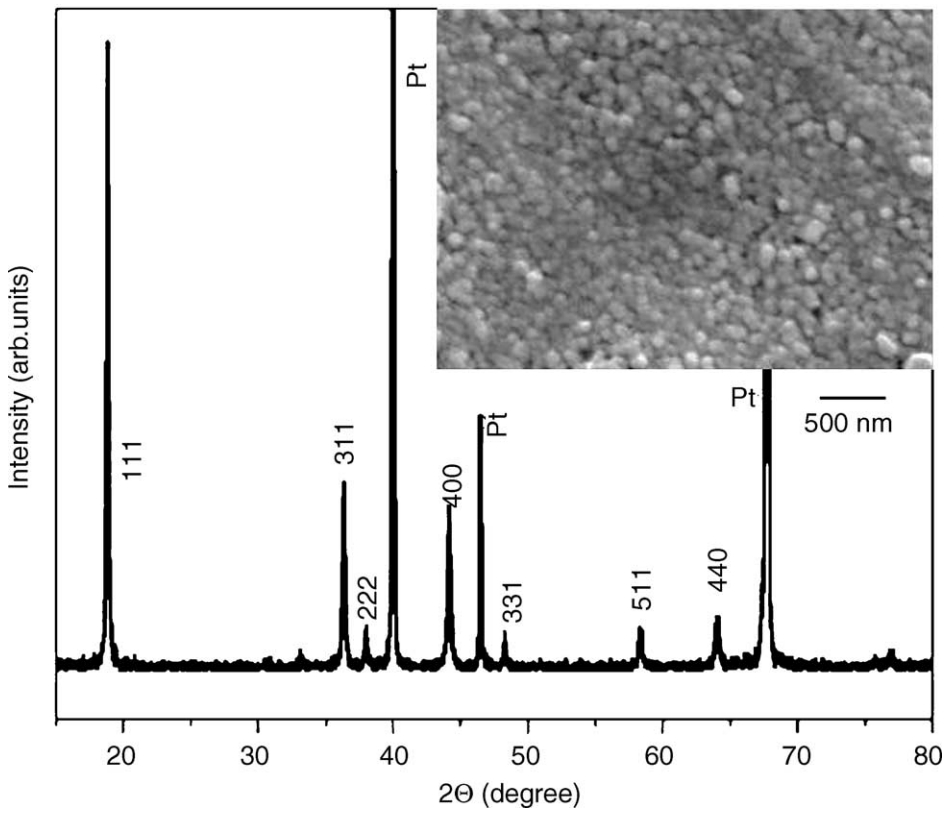

Fig. 1. X-ray diffractograms of $Li_{1.40}Mn_{2.0}O_4$ thin film on platinum substrate. The inset shows the scanning electron micro-graph of the thin film surface.

that the diffusion coefficient was reduced appreciably after the repeated cycling. It has been argued that the reduced Li ion diffusivity, due to the formation of a SEI layer on the thin film electrode causes the observed capacity fading.

2. Experimental

To prepare the precursor solution for thin film deposition, lithium acetate and manganese acetate (in the molar ratio of 1.40:2) were co-dissolved in warm ethyl-hexanoic acid through continuous stirring. Films were deposited using precursor sol of various excess lithium contents and it was found that addition of 20–40 at % excess lithium was always necessary to obtain phase pure (cubic spinel with no other impurity phase/(s)) LMO thin films. The molar concentration of precursor solution was maintained $\sim$0.5 M L^{-1}, and it was spin coated on to a platinum substrate at 3000 rpm for 5 s. Just after deposition, the films were directly inserted into a pre-heated furnace kept at 400 °C and fired for 5 min to remove the associated organics. The coating and firing schedule was repeated for 10 times to yield films about 0.5 μm thick. Thicker films (>1 μm) were deposited either by increasing the concentration of coating sol or by increasing the number of coatings. After final firing, these films were annealed at 700 °C for 120 min for crystallization into cubic spinel structure. The firing and annealing temperatures were decided on the basis of differential thermal analysis of gel-derived powder of the precursor sol [15]. X-ray diffraction was used to analyze the phase formation behavior, scanning electron microscopy was used to study the surface morphology and cross sectional SEM micro-graphs were used to estimate the film thickness. Fig. 1 shows the X-ray diffractograms of the process optimized $Li_{1.40}Mn_2O_4$ film. All the indexed diffraction peaks were from cubic spinel structure. The inset of the figure shows its dense surface morphology and homogenous grain size distribution with average size about 100 nm. The electrochemical properties of these films were evaluated in a three electrodes open beaker cell using Li foil both as counter and reference electrodes and LMO thin film on platinum substrate as working electrode. The electrolyte solution was 1 M $LiPF_6$ salt mixed with ethylene carbonate (EC) and di-methyl carbonate (DMC) in 1:2 molar ratio. All the electrochemical experiments were performed inside moisture-controlled glove box. The films were about 0.5 μm thick unless specified otherwise and the electrode area inside the electrolyte solution was 0.33 cm^2. A computer-controlled potentiostat–galvanostat system was utilized for the electrochemical measurements. The cyclic voltammograms were recorded at various voltage scan rate (v) ranging 0.2–1 mV s^{-1} in a cut-off limits of 4.2–3.4 V. Potential step chronoamperometry measurements were performed by applying a potential step from 3.93 to 4.10 V versus Li/Li^+, i.e. the potential corresponding to the first cathodic peak on CV plot. Both the CV and chronoamperometry data were analyzed to estimate diffusion coefficient of Li^+ ions at room temperature. The charge–discharge measurements were performed at constant current densities ranging 30–180 μA cm^{-2} in a cut-off voltage limit of 4.3–3.4 V Li/Li^+. The discharge capacity and the rate capability were estimated from these measurements. The charge–discharge measurements were repeated to estimate the discharge capacity as a function of the number of switching cycles (cycleability).

3. Results and discussions

Fig. 2(a) shows the charge–discharge characteristics of $Li_{1.40}Mn_2O_4$ thin films (having thickness >1 μ) at current densities ranging 30–90 μA cm^{-2} in a cut-off voltage in the range 3.4–4.2 V. As shown in this figure, the discharge

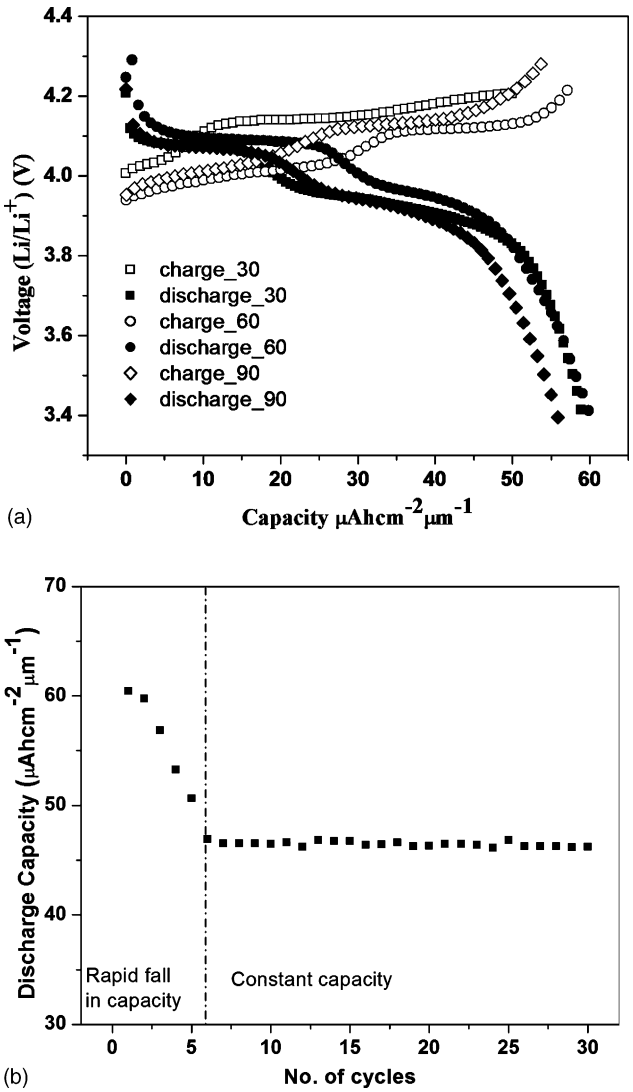

Fig. 2. (a) Charge–discharge characteristics of $Li_{1.40}Mn_{2.0}O_4$ thin films at different current densities in the cut-off voltage range of 4.2–3.4 V Li/Li^+. (b) Cycleability of $Li_{1.40}Mn_{2.0}O_4$ thin film at a discharge current density of 180 μA cm^{-2} in the cut-off voltage limit between 4.2 and 3.4 V Li/Li^+.

capacity, irrespective of the load current density, is close to the theoretical capacity (~64 μAh cm^{-2} μm^{-1}) of spinel lithium manganate. Irrespective of the load current density, these films exhibits >90% Coulombic efficiency. The two distinct plateaus in the 4 V range are due to the ordering of Li^+ in the tetrahedral sites or Mn ions in the octahedral sites, which corresponds to a cubic-to-cubic transition. No significant change of the discharge capacity was observed with further increase of the load current density. Thus, the discharge capacity of 0.5 μm thick LMO film, measured at 180 μA cm^{-2}, was about 50 μAh cm^{-2} μm^{-1}. However, in this case the plateaus were not very distinct (not shown). These results indicate that the sol–gel grown films have excellent rate capabilities, i.e. there is no appreciable reduction of the discharge capacity with the increase in load current densities. Fig. 2(b) shows the cycleability of 0.5 μm thick LMO film in the cut-off voltage range of 3.4–4.2 V Li/Li^+. As shown in the figure, the discharge capacity drops significantly within first few cycles (marked by dash-dotted line in the figure) and marginally changes thereafter with repeated charge–discharge cycles. The electrochemical properties of our solution-derived films are compared with the properties of LMO thin films deposited by other techniques (Table 1). From the table, it is clear that our solution derived LMO thin films have excellent discharge capacity and rate capabilities in the 4 V range. Since the discharge capacity and the cycleability of LMO thin films in 4 V range depends on various factors including the synthesis route, crystallinity, nature of electrolyte, anode used, and discharge current densities, etc [16–21], it is difficult to make any effective comparison of the electrochemical performance of LMO thin films synthesized in various laboratories. It is interesting to note that as compared to a liquid electrolyte cell, the all-solid-state cell usually exhibits superior discharge capacity, excellent cycleability, and rate capabilities [19–22]. Considering this fact, it seems that the interaction between liquid electrolyte and the thin film electrode could be related to the observed capacity fading in case of the present study. Having grain size of our LMO films in nano-range, the surface area of the exposed thin film dipped in the electrolyte is very high; and therefore, any such interaction reaction (between the electrolyte and thin film surface) during the charge and discharge cycle will be much faster as compared to films with larger grain size. Recently it has been reported that LMO based composite electrodes in any Li salt containing EC–DMC based liquid electrolytes are indeed masked by solid electrolyte interface (SEI) film composed by Li_2CO_3, and during subsequent electrochemical cycling, the $LiCO_3$ film dissolves and replaced by electrolyte related surface species and salt reduction products that eventually deteriorate Li ion intercalation [23]. The formation of SEI layer strongly depends on the temperature, electrolyte as well as electrode composition; however, the exact mechanism of their formation and nature of growth still remains debatable [24,25].

Since the formation of any such surface layer could eventually retard the Li ion diffusion in the cathode thin films, the rapid capacity fading during the initial charge–discharge cycles is thought to be related to the formation of a solid electrolyte interface film on the thin film electrode. From the studies on the nature and the growth kinetics of the SEI films, it is becoming clearer that the formation of such surface films often significantly reduce the electronic conductivity of the LMO particles and consequently causes capacity loss. In order to gain better understanding on these aspects, we have performed CV and PSCA measurements to investigate the kinetics of Li^+ ion in the solution derived LMO thin films. It is known that the change in peak shape with sweep rate reflects the kinetics of Li intercalation/deintercalation at the electrode/electrolyte interface and/or rate of Li^+ dif-

Table 1
Summary of the electrochemical properties of $LiMn_2O_4$ thin films

Deposition	Electrolyte/anode	Thickness (μm)	Discharge capacity (4 V) (μAh cm^{-2} μm^{-1})	Cycleability (4 V) (discharge current density)	References
PLD	1 M $LiClO_4$ in propylene carbonate/Li	0.3	49	Rapid capacity fading in initial cycles, poor rate capability with the increase in current density (10 μA cm^{-2})	[16]
PLD	1 M $LiPF_6$ in EC: DMC (1:2)/Li	0.3	66	0.03–0.17%/cycle up to 25 cycles (35 μA cm^{-2})	[17]
Sol–gel	1 M $LiClO_4$ in PC	0.2	32	No fading from 5 to 100 cycles (100 μA cm^{-2})	[18]
Rf sputtering	LIPON/Li (all solid-state configuration)	0.3	48	About 4% capacity fading in 100 cycles (100 μA cm^{-2})	[19]
Sol–gel	1 M $LiClO_4$ in EC: DMC (1:1)/Li	1.0	60	No fading up to 50 cycles (50 μA cm^{-2})	[20]
Rf sputtering	1 M $LiPF_6$ in EC:DMC/a-Si		24	Rapid fading in the initial cycles, 67% retained after 100 cycles (10 μA cm^{-2})	[21]
Solution growth	1 M $LiPF_6$ in EC:DMC/Li	0.5	49	Rapid fading during the initial cycles (180 μA cm^{-2})	This work
		>1.0	64		

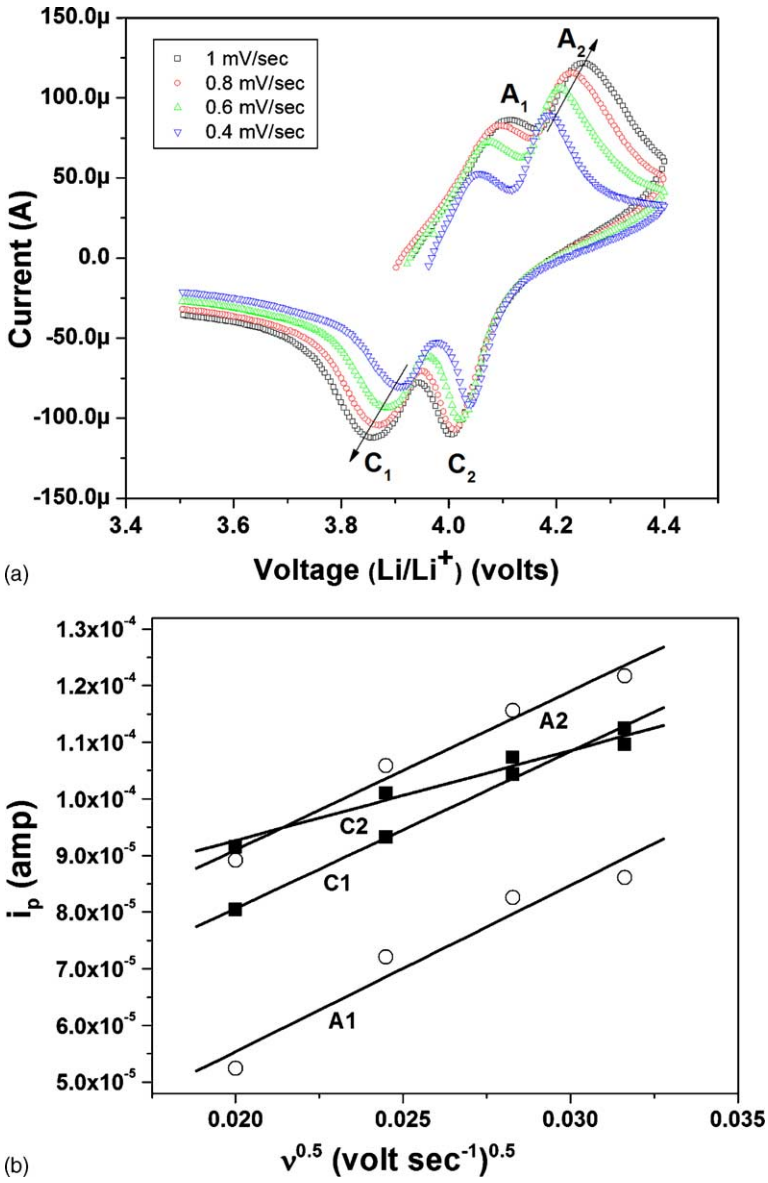

Fig. 3. (a) Cyclic voltammograms of $Li_{1.40}Mn_{2.0}O_4$ thin films at various voltage scan rates, v. (b) Plot of peak current (i_p) of the cyclic voltammograms vs. $\sqrt{v}$. The linear fitting was according to Eq. (1) (see text).

fusion in the film [26]. Fig. 3(a) shows the cyclic voltammograms of $LiMn_2O_4$ thin films recorded different scan rate (0.4–1 mV s^{-1}) in the voltage range of 3.4–4.3 V Li/Li^+. The anodic (A) peaks during charging are due to the two-step Li^+ de-intercalation from the cathode, whereas the cathodic (C) peaks are due to the Li^+ intercalation into the thin films cathode. As evident in Fig. 3, as v increases, cathodic and anodic peaks move to lower and higher potential, respectively (indicated by small arrows) with the increase of the magnitude of i_p. Levi and Aurbach [27] suggested that usually two limiting ranges of v can be observed on experimental CV measured from thin Li-insertion electrodes; in the case of semi-infinite and finite diffusion, the peak current (i_p) is proportional to the square root of the scan rate (v) and accordingly for any separate red–ox reaction in the plotted CV curve may be expressed as [28]

$$i_p = 2.69 \times 10^5 n^{3/2} A D^{1/2} v^{1/2} \Delta C_o \quad (1)$$

where n is the number of electrons per reaction species (for Li^+ it is 1), A is the dipped area of the film into the electrolyte solution, D_{Li} is the diffusion coefficient of Li in the film, ΔC_o is the change in Li concentration corresponding to the specific electrochemical reaction. At very slow scan rate Li^+ accumulates in the bulk of the thin film and in this case the peak current (i_p) varies linearly with the scan rate (v). In the present case, as shown in Fig. 3(b) i_p is indeed proportional to $\sqrt{v}$ confirming a diffusion-controlled behavior. From the slope of the linear fit, we have calculated the diffusion coefficients corresponding to A1, A2, C1, and C2 electrochemical

reactions to be 7.59×10^{-12}, 6.88×10^{-12}, 6.76×10^{-12}, and 2.23×10^{-12} $cm^2\ s^{-1}$, respectively. The order of diffusion coefficients for anodic and cathodic reactions remains the same, which indicates excellent reversibility of the intercalation process. However, using CV only the average values of D_{Li} ($\sim 5.86 \times 10^{-12}$ $cm^2\ s^{-1}$) could be obtained. A much better resolution of the dependence of D_{Li} on the electrode potential might be obtained by the use of the potential step chronoamperometry technique. In this study, we have applied potential from 3.9 to 4.10 V (corresponding to the second cathodic peak, C2 in the C–V plot) and we measured current as a function of time. The resultant current (i) versus time (t) plot is shown in Fig. 4(a). Following the general features of the electrochemical intercalation reaction, we would expect the appearance of different time domains corresponding to the separate steps of the entire intercalation process. As reported by Levi et al. [29], various kinetic regions of the intercalation process could be identified by plotting $it^{1/2}$ versus log(t). One such plot for the virgin thin film electrode is shown in Fig. 4(b). The region marked 'A' corresponds to the interfacial charging of cathode electrolyte interface. The $it^{1/2}$ values remain almost constant in the region 'B' where semi-infinite planar diffusion of Li^+ ions takes place in the cathode. In the region 'C', finite Li^+ diffusion occurs in the cathode. In this time domain the functional dependence of current (i) with time (t) can be expressed by the following equation [30]

$$\ln(i) = \ln\left(\frac{2\Delta Q D_{Li}}{d^2}\right) - \left(\frac{\pi^2 D_{Li}}{4d^2}\right)t \quad (2)$$

where ΔQ is the amount of charge injected into the electrode, D_{Li} is the diffusion coefficient of Li; d is the thickness of the

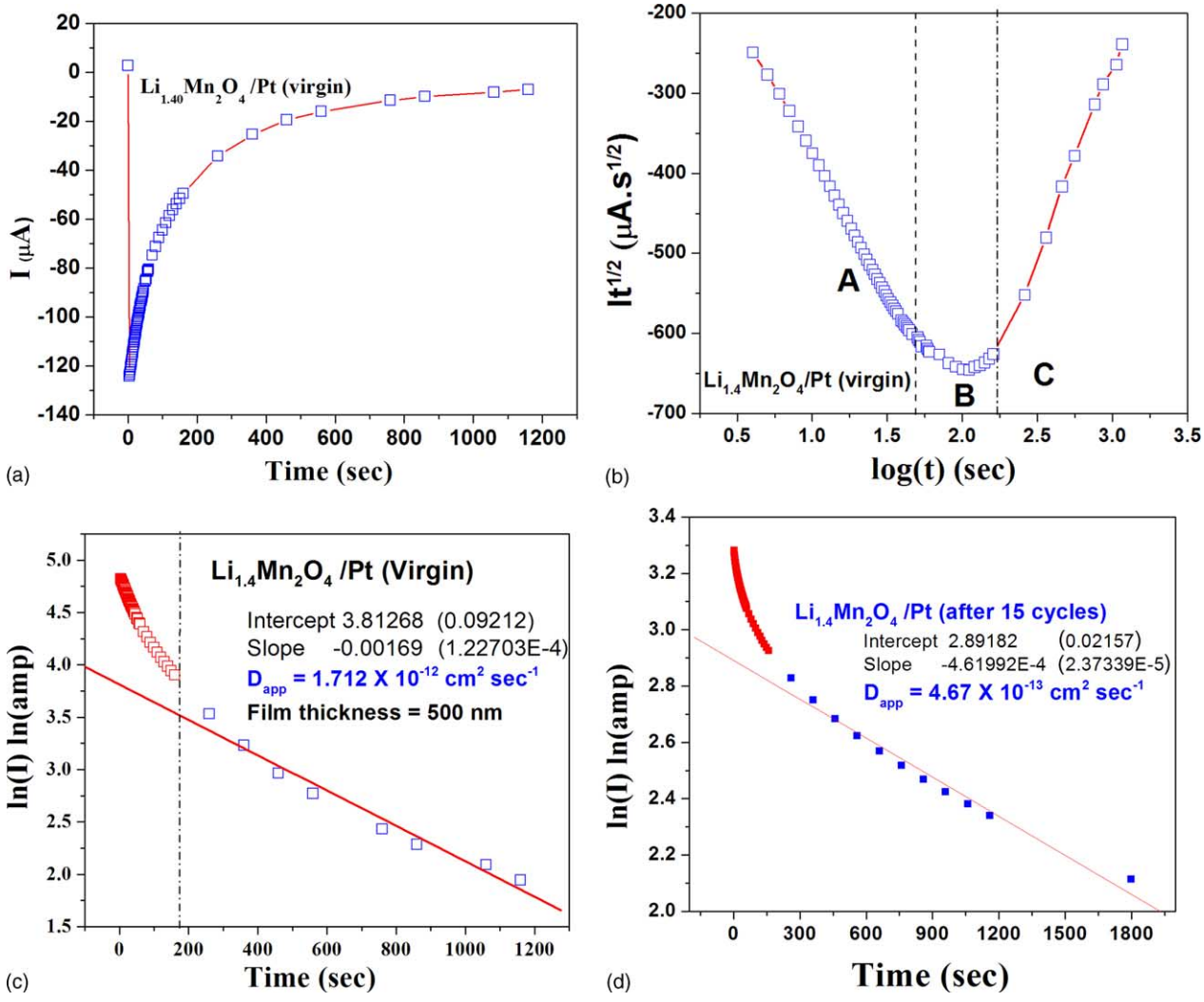

Fig. 4. (a) Current transient of the virgin $Li_{1.40}Mn_{2.0}O_4$ film from the PSCA measurements in the potential range 3.9–4.10 V Li/Li^+. (b) Plot of $it^{1/2}$ vs. log(t) derived from the PSCA measurements of the virgin film. The different kinetic regions of the intercalation process are marked in the figure as A, B, and C (see text). (c) Plot of ln(i) vs. t from the PSCA measurements of the virgin film. The linear fit is according to the Eq. (2). The Li ion diffusion coefficient in the virgin thin film electrode was calculated from the slope of the linear fit (see text). (d) Plot of ln(i) vs. t from the PSCA measurements of the electrochemically cycled film after 15 charge–discharge cycles. The linear fit is according to the Eq. (2). The Li ion diffusion coefficient in the cycled electrode was calculated from the slope of the linear fit.

Table 2
Comparison of D_{Li} (X 10^{-12} cm^2 s^{-1}) in various forms of virgin $LiMn_2O_4$ cathodes

Method used for D_{Li} estimation	Composite with binder and conducting agents	Single crystal	Porous particle (8–21 μm) (aggregates of nano-crystallites)	Thin film
CV				5.86 (virgin), this work
PSCA				1.71 (virgin), 0.47 (after cycling), this work
CV	2200 [10]			35 [16]
PSCA	1000 [11]	14.8 [31]	360 [32]	3.98 [33] 6.1 [34]
EIS[a]			250 [32]	19 [17]
GITT[b]				25 [33]

[a] Electrochemical impedance spectroscopy.
[b] Galvanostatic intermittent titration technique.

film. As marked by dash-dotted line in Fig. 4(b), the time domain that follows Eq. 2 was estimated to be ≥160 s. Fig. 4(c) shows the plot of ln(*i*) versus *t*, and in the time domain $t >$ 160 s the data were linear fitted according to Eq. (2) and the Li ion diffusion coefficient in the virgin thin film LMO cathode, calculated from the slope ($\sim\pi^2 D_{Li}/4d^2$), was 1.71 × 10^{-12} cm^2 s^{-1}. Similar chronoamperometry measurements and subsequent analyses were also performed on 15 times cycled (at constant current density of 180 μA cm^{-2} in the cut-off voltage range 4.3–3.4 V) LMO thin film electrodes and in this case the Li ion diffusion coefficient estimated to be 4.67 × 10^{-13} cm^2 s^{-1} (Fig. 4d). Limited literature reports are available on the kinetic analyses of Li ion diffusion in $LiMn_2O_4$. The available apparent chemical diffusion coefficients (D_{Li}) of Li ion in single crystal, single particles with aggregates of crystallites, composite electrodes, and thin films of lithium manganates have been compared in Table 2. Since the diffusion coefficient varies with the electrode potential, for any effective comparison the Li/Li^+ potential should be of similar range. From the table, it is clear that porous the electrode better is the Li ion diffusion; however, the kinetic data on the porous composite electrodes (containing active LMO, binder, and conducting agent) [10,11] are not very reliable and do not reflect the characteristics solely due to the active materials. In that respect, thin films are indeed an ideal system to study the diffusion kinetics as the Li ion diffusion takes place either through the grain or the grain boundary regions. Note that in the present case the Li ion diffusion coefficient is reduced by about an order of magnitude after the repeated charge–discharge cycling which is thought to be due to the formation of SEI film on the thin film surface which eventually retards the Li ion diffusion into the electrode which lead to the observed capacity fading. The SEI layer is formed during the initial charge–discharge cycles which eventually leads to the drop in capacity; however, with progressive charge–discharge cycling the capacity is marginally reduced. Since these films have nano-size grains with large specific surface area, they may be very reactive to the liquid electrolyte during charge–discharge cycles to form SEI layer [23–35]. However, the nature of the SEI film and their growth kinetics is not clearly understood at this stage and further research is required to understand this.

4. Conclusions

In the present work, we have successfully synthesized nano-crystalline lithium manganate thin films by solution growth technique. Excess lithium addition was found necessary to obtain thin films with the cubic spinel structure. These films had dense surface morphology with uniform grain size distribution. In the 4 V range, the films had excellent discharge capacity (49–64 μAh cm^{-2} μm^{-1}) and high Coulombic efficiency, measured at a wide variation of current densities (30–180 μA cm^{-2}). To understand the rapid capacity fading at high discharge current densities, we have estimated the Li ion diffusion coefficient by analyzing the data of the CV as well as PSCA measurements. The virgin electrode had Li ion diffusion coefficient in the range of (1–6) × 10^{-12} cm^2 s^{-1}. After repeated charge discharge cycling, the estimated diffusion coefficient dropped down to 0.47 × 10^{-13} cm^2 s^{-1}. Since the nano-crystalline thin film surface is very reactive to the liquid electrolyte, possibly a SEI film forms on the electrode, which eventually retards the Li ion diffusion leading to the observed capacity fading. Further research is necessary to investigate the nature, formation, and growth kinetics of such surface layers. The utilization of solid-state electrolytes, with high Li ion conductivity, may be effective to eliminate any such SEI layer formation and improve the electrochemical characteristics of these nano-crystalline thin film electrodes.

Acknowledgements

The above research work was partially supported by the research grants from DoE (# DE-FG02-01ER45868) and NASA (# NAG3-2676) Glenn research center. XRD and SEM measurements were carried out utilizing the facilities at the Materials Characterization Center (MCC) of UPR.

References

[1] J.M. Tarascon, D. Guyomard, Electrochim. Acta 38 (1993) 1221.
[2] C.R. Sides, N.L. Charles, J. Patrissi, B. Scorosati, C.R. Martin, Bull. Mat. Res. Soc. August (2002) 604.
[3] N. Li, C.J. Patrissi, G. Che, C.R. Martin, J. Electrochem. Soc. 147 (2000) 2044.
[4] K. Matsuda, I. Taniguchi, J. Power Sources 132 (2004) 156.

[5] M.G. Lazarraga, S. Mandal, J. Ibanez, J.M. Amarilla, J.M. Rojo, J. Power Sources 115 (2003) 315.
[6] C.J. Curtis, J. Wang, D.L. Schulz, J. Electrochem. Soc. 151 (2004) 590.
[7] A. Odani, A. Nimberger, B. Markovsky, E. Sominski, E. Levi, V.G. Kumar, M. Motiei, A. Gedanken, P. Dan, D. Aurbach, J. Power Sources 119–121 (2003) 517.
[8] H.J. Choi, K.M. Lee, G.H. Kim, J.G. Lee, J. Am. Ceram. Soc. 147 (2001) 242.
[9] P. Lucas, C.A. Angell, J. Electrochem. Soc. 147 (2000) 4459.
[10] J. Barker, R. Pynenburg, R. Koksbang, J. Power Sources 52 (1994) 185.
[11] D. Guyomard, J.M. Tarascon, J. Electrochem. Soc. 143 (1996) 1827.
[12] K. Dokko, M. Mohamedi, M. Umeda, I. Uchida, J. Electrochem. Soc. 150 (2003) A 425.
[13] L. Croquennec, P. Deniard, R. Brec, P. Biensan, M. Broussely, Solid State Ionics 89 (1996) 127.
[14] J.B. Bates, N.J. Dudney, B. Neudecker, A. Ueda, C.D. Evans, Solid State Ionics 135 (2000) 33.
[15] S. Nieto, S.R. Das, S.B. Majumder, R.S. Katiyar, Surf. Coat. Technol. 177 (2004) 60.
[16] K.A. Striebel, C.Z. Deng, S.J. Wen, E.J. Cairns, J. Electrochem. Soc. 143 (1996) 1821.
[17] K.A. Striebel, A. Rougier, C.R. Horne, R.P. Reade, E.J. Cairns, J. Electrochem. Soc. 146 (1999) 4339.
[18] Y.J. Park, J.G. Kim, M.K. Kim, H.T. Chung, W.S. Um, M.H. Kim, H.G. Kim, J. Power Sources 76 (1998) 41.
[19] Y.S. Park, S.H. Lee, B.I. Lee, S.K. Joo, Electrochem. Solid State Lett. 2 (1999) 58.
[20] Y.H. Rho, K. Kanamura, T. Umegaki, J. Electrochem. Soc. 150 (2003) A107.
[21] K.L. Lee, J.Y. Jung, S.W. Lee, H.S. Moon, J.W. Park, J. Power Sources 130 (2004) 241.
[22] N.J. Dudney, J.B. Bates, R.A. Zuhr, S. Young, J.D. Robertson, H.P. Jun, S.A. Hackney, J. Electrochem. Soc. 146 (1999) 2455.
[23] D. Aurbach, K. Gamolsky, B. Markovsky, G. Salitra, Y. Goefer, U. Heider, R. Oesten, M. Schmidt, J. Electrochem. Soc. 147 (2000) 1322.
[24] S.S. Zhang, K. Xu, T.R. Jow, J. Electrochem. Soc. 149 (2002) A1521.
[25] Y. Matsuo, R. Kostecki, F. McLarnon, J. Electrochem. Soc. 148 (2001) A687.
[26] A. Rougier, K.A. Striebel, S.J. Wen, E.J. Cairns, J. Electrochem. Soc. 145 (1998) 2975.
[27] M.D. Levi, D. Aurbach, J. Electroanal. Chem. 421 (1997) 79.
[28] A.J. Bard, L.R. Faulkner, Electrochemical Methods: Fundamentals and Applications, Wiley, New York, 1980, p. 218.
[29] M.D. Levi, E.A. Levi, D. Aurbach, J. Electroanal. Chem. 421 (1997) 89.
[30] C.J. Wen, B.A. Boukamp, R.A. Huggins, W. Weppner, J. Electrochem. Soc. 126 (1979) 2258.
[31] K. Dokko, M. Nishizawa, M. Mohamedi, M. Umeda, I. Uchida, J. Akimoto, Y. Takahashi, Y. Gotoh, S. Mizuta, Electrochem. Solid-State Lett. 4 (2001) A151.
[32] K. Dokko, M. Mohamedi, M. Umeda, I. Uchida, J. Electrochem. Soc. 150 (2003) A425.
[33] D. Shu, K.Y. Chung, W.I. Cho, K.B. Kim, J. Power Sources 114 (2003) 253.
[34] M. Nishizawa, T. Uchiyama, K. Dokko, K. Yamada, T. Matsue, I. Uchida, Bull. Chem. Soc. Jpn. 71 (1998) 2011.
[35] D. Shu, K.Y. Chung, W.I. Cho, K.B. Kim, J. Power Sources 114 (2003) 253.